

# Echoes of the past: ultra-high energy cosmic rays accelerated by radio galaxies, scattered by starburst galaxies

AR Bell<sup>1,2\*</sup>, JH Matthews<sup>3</sup>

<sup>1</sup>University of Oxford, Clarendon Laboratory, Parks Road, Oxford OX1 3PU, UK

<sup>2</sup>Central Laser Facility, STFC Rutherford Appleton Laboratory, Harwell Oxford, Oxfordshire OX11 0QX, UK

<sup>3</sup>Institute of Astronomy, University of Cambridge, Madingley Road, Cambridge, CB3 0HA, UK

28 February 2022

## ABSTRACT

We suggest that the hotspot of ultrahigh energy cosmic rays (UHECR) detected by the Telescope Array (TA) from the direction of M82 might be the echo of UHECR emitted by Centaurus A in a more powerful phase approximately 20Myr ago. Echoes from other starburst galaxies may contribute to the UHECR flux at the Earth.

**Key words:** cosmic rays, acceleration of particles, radio galaxies, starburst galaxies

## 1 INTRODUCTION

The origin of ultrahigh energy cosmic rays (UHECR) remains one of the most challenging unknowns in astrophysics. Directional data from the Pierre Auger Observatory (PAO) in the southern hemisphere and the Telescope Array (TA) in the northern hemisphere give hope that we are close to identifying their source. The Hillas (1984) parameter  $E_{\max} = ZuBR$  for the maximum attainable cosmic ray (CR) energy expressed in eV, where  $u$ ,  $B$  and  $R$  are the characteristic velocity, magnetic field and spatial scale and  $Ze$  is the UHECR charge, places telling constraints on the nature of the source. As pointed out by many authors (Lovelace, 1976; Waxman, 1995; Blandford, 2000; Lemoine & Pelletier, 2010), the Hillas parameter is related to the magnetic power  $P_{\text{mag}}$  of the source:  $ZuBR = Z(u\mu_0 P_{\text{mag}})^{1/2}$  where  $P_{\text{mag}} = uR^2 B^2 / \mu_0$ . This relation can be inverted to give a lower limit on the magnetic power,  $P_{\text{mag}} > E_{\max}^2 / (Z^2 u \mu_0)$ . The total source power must exceed this because (i) the magnetic energy is only one part of the total energy, (ii) the power channeled through the accelerating structure, probably but not necessarily a shock, is a fraction  $\xi$  of the total source power. Taking characteristic values suitable for radio galaxies, the total power can be estimated:

$$P_{\text{total}} \sim 2 \times 10^{44} Z_6^{-2} E_{100}^2 (u/0.3c)^{-1} \xi_{0.1}^{-1} \text{ erg s}^{-1} \quad (1)$$

where  $Z = 6Z_6$ ,  $E_{\max} = 100E_{100}$  EeV,  $\xi = 0.1\xi_{0.1}$ . Taken together, the Hillas condition and the related power requirement restrict the range of possible sources of UHECR. The stringent power requirement points to radio galaxies (RG) or gamma-ray bursts (GRB) as possible contenders.

GRB easily reach the required power due to the short time in which energy is released, but there are many issues that question the viability of GRB as an explanation of UHECR origins. These issues relate to limits placed by the expected associated neutrino fluxes, radiation losses during UHECR acceleration and escape, host galaxy metallicity, UHECR composition and the ability of GRB to

provide the entire UHECR flux. (Hillas 1984, Waxman & Bahcall 1997, 1998, Aharonian et al 2002, Ptitsyna & Troitsky 2010, Dermer 2011, Baerwald et al 2015, Anchordoqui 2018, Zhang et al 2018, Alves Batista et al 2019, Boncioli 2019, Samuelsson et al 2019; Heinze et al 2020, Rudolph et al 2021). An additional difficulty with GRB as a producer of UHECR is that relativistic shocks are not good accelerators to ultra-high energies (Bell et al 2018).

Here we focus on RG as a natural source of UHECR because they are large, powerful, and long-lived. Also, radiative losses are not a strong limitation if acceleration takes place in the lobes where magnetic and radiation energy densities are relatively small. RG display features such as shocks, shear flows, and magnetic reconnection that are known to be suitable for CR acceleration.

Cygnus A is a clear candidate for UHECR production since it far exceeds the power requirement (Eichmann et al, 2018), but its distance of 237Mpc (Persic & Rephaeli 2020) counts against it because (i) UHECR from Cygnus A are unlikely to arrive at the Earth anisotropically without scattering since a magnetic field of only 0.03nG is needed to make their Larmor radius smaller than the distance to Cygnus A (ii) even without scattering, the UHECR travel time from Cygnus A is many times the loss time due to the Greisen–Zatsepin–Kuzmin (GZK; Greisen 1966; Zatsepin & Kuz'min 1966) effect and photodisintegration (e.g. Stecker & Salamon 1999, Hooper, Sarkar & Taylor 2007).

In fact, powerful FRII galaxies are rare within the local GZK volume (Massaglia 2007, van Velzen et al 2018). FRI radio galaxies are more populous, and radio galaxies at the FRI/FRII boundary have powers close to  $P_{\text{total}}$  as given in equation (1). The most obvious FRI candidate is Centaurus A (Cen A) which is nearby and estimated to have a cavity power of  $10^{44} \text{ erg s}^{-1}$  (Hardcastle et al 2009, O'Sullivan et al 2009, Cavagnolo et al 2010, van Velzen et al 2012, Matthews et al 2019). The case for Cen A is strengthened by the coincidence of Cen A with the brightest UHECR hotspot detected by PAO (Aab et al 2018) and the apparent need for local UHECR sources (Guedes Lang et al 2020). PAO also detects a weaker hotspot with weaker statistical significance in the direction of the FRI galaxy Fornax A which has

\* E-mail: Tony.Bell@physics.ox.ac.uk

similar characteristics to Cen A (Matthews et al 2018), including evidence of variability (Mackie & Fabbiano 1998, Maccagni et al 2020).

The arrival directions of UHECRs favour starburst galaxies or AGN as likely sources. Aab et al (2018) and Bister et al (2021) find a statistically significant correlation of PAO arrival directions with active galaxies, but find an even stronger correlation with starburst galaxies. Further evidence pointing toward starburst galaxies and away from radio galaxies is the lack of a powerful radio galaxy in the direction of the UHECR hotspot detected by TA in the northern hemisphere. An analysis of the TA data for associations with starburst galaxies is not statistically significant (Abbasi et al 2018). However, the TA hotspot lies in the direction of the nearby strong starburst galaxy M82. Hence starburst galaxies appear to be a strong candidate. However, their powers reach typically  $10^{42} \text{erg s}^{-1}$  and the characteristic wind velocity in a starburst region is  $\sim c/100$ , (Heckman, Armus & Miley 1990; Anchordoqui 2017; Romero, Muller & Roth 2018, Matthews et al 2020), so they fail to reach the power condition (equation 1) for a source of UHECR. We therefore proceed by ruling out starburst galaxies as a direct source of UHECR despite their statistical correlation with UHECR arrival directions. The possibility remains that UHECR are produced by GRB associated with starburst galaxies.

Here we explore the possibility that starburst galaxies are instead reflectors of UHECR without themselves being a source of UHECR. We propose that the environs of starburst galaxies are regions of enhanced scattering that diffusively reflect UHECR back towards the Earth after their initial acceleration by Cen A. In particular we propose that the TA hotspot is associated with the M81 galaxy group that contains the prominent starburst galaxy M82. M82 is close by at a distance of 3.7Mpc from the Earth, which is similar to the distance of Cen A from the Earth.

Starburst galaxies can generate a large magnetic field, 100–300 $\mu\text{G}$ , in the central kpc (Domingo-Santamari & Torres 2005, de Cea del Pozo, Torres & Marrero 2009, Anchordoqui 2018) which may be carried 100s kpc into the surrounding medium by the superwind. In a spherical wind expanding at constant velocity, a frozen-in magnetic field decays as the inverse of the distance. Hence there is good reason to think that the magnetic field may easily exceed the  $\sim 10\text{nG}$  needed to make the UHECR Larmor radius smaller than the wind radius should it reach 1Mpc. A magnetic field of  $\sim 100\text{nG}$  at 100 kpc would similarly be sufficient for UHECR to be scattered in a starburst wind.

The TA hotspot extends an angular diameter of 20 – 30° across the sky (Kawata et al 2015, Anchordoqui 2018), corresponding to a physical radius of 0.6 – 1Mpc at the distance of M82. This is consistent with the analysis of di Matteo et al (2019) who identify the hotspot by drawing around it a circle of radius 15° corresponding to 1Mpc. The size of the hotspot is due to a combination of UHECR scattering and the size of the source, and the UHECR numbers are not sufficient to clearly define the shape and size of the hotspot. In our model, we assume that M82 and the M81 group present to UHECR an optically thick sphere of radius 800kpc. The radius of 800kpc then corresponds to the distance to which the starburst superwind affects the surrounding intergalactic medium to produce an enhanced magnetic field. An extension of this radius into the surrounding medium is consistent with recent observations (Wilde et al 2021) given that starburst winds are stronger than typical galactic winds.

Other factors commensurate with an enhanced magnetic field in the M81 group are the presence of a second starburst galaxy NGC3077 in the group and dynamo action arising from motions as galaxies in the group interact with each other.

Cen A, M82 and the Earth form an approximately isosceles triangle with M82 and Cen A both about 3.7Mpc from the Earth as shown in figure 1. The corresponding distance between Cen A and M82 is 6.4Mpc. The UHECR travel time from Cen A to the Earth via M82 is longer by 21Myr, which means that the UHECR luminosity of the M81 group reflects the luminosity of Cen A 33Myr ago as it would have appeared at the Earth 21Myr ago.

As discussed by Matthews & Taylor (2021), the time variation of UHECR production by radio galaxies depends on variation in accretion onto the central black hole, the hydrodynamic response of the jets and lobes, the sensitivity of the acceleration process to the presence of shocks and turbulence, and the residence time of UHECR in the lobes. Matthews & Taylor (2021) consider a jet power that varies according to a flicker noise power spectrum with a log-normal distribution of jet powers, motivated by the chaotic cold accretion model of Gaspari et al. (2017) and numerical simulations of AGN fuelling (Yang & Reynolds 2016; Beckmann et al 2019); these studies suggest that variation in jet power by orders of magnitude on a 20Myr timescale is reasonable even before considering the individual history of Cen A. UHECR production can be especially spasmodic due to the need to exceed the power threshold. Conditions for UHECR acceleration may exist only during peak periods of activity with CR failing to reach UHECR energies during quiescent periods. In our picture, Cen A is in a relatively inactive state at the present time with weak UHECR production compared with 20 Myr ago when it was more active. We note that this timescale is comparable to the spectral age of the synchrotron electrons in the giant lobes, estimated to be  $\sim 25$  Myr by Hardcastle et al (2009).

From repeated application of the inverse square law, the UHECR flux arriving at the Earth via M82 is about 100× smaller than the flux arriving directly from Cen A if the same number of UHECR are released in the directions of M82 and the Earth. This is confirmed by figure 2 below where we show the results of a Monte Carlo calculation.

It is not unreasonable that the UHECR luminosity of Cen A over longer timescales of 10sMyr should be greater than its present luminosity. We have previously suggested (Matthews et al. 2018, 2019) that the giant inflated lobes of Cen A act as UHECR reservoirs and that the present flux of UHECR direct from Cen A is the leakage from the lobes of UHECR accelerated during past active episodes. This would explain how UHECR can now be arriving from Cen A when the present jet power of  $\sim 10^{43} \text{erg s}^{-1}$  (Russell et al 2013, Wykes et al 2013, Matthews et al 2018) falls short of that required by equation (1). A further indication of past enhanced activity is that the size and energy content of the large radio lobes is large in comparison with the present weak radio jets that extend only a small distance into the lobes.

From figure 4 of di Matteo et al 2019, we estimate that the UHECR flux arriving at the Earth via M82 above 53EeV is the equivalent of an isotropic UHECR source with power  $3 \times 10^{39} \text{erg s}^{-1}$  at the position of M82. Allowing for the factor of 100 discussed above from double application of the inverse square law, the UHECR power of Cen A as it would have been observed at the Earth 21Myr ago was  $\sim 3 \times 10^{41} \text{erg s}^{-1}$ , which is 100 – 300× its UHECR power as observed now.

Further indications that the UHECR power of Cen A might have been greater in the past are (i) the present UHECR (energy greater than 55EeV) power of Cen A, estimated to be  $2 \times 10^{39} \text{erg s}^{-1}$  (Joshi et al 2018), is very much smaller than the Eddington luminosity of  $5 \times 10^{45} \text{erg s}^{-1}$  corresponding to its central black hole mass of  $5.5 \times 10^7$  solar masses (Capellari et al 2009) (ii) the large energy content,  $10^{59} - 10^{60} \text{erg}$  of the lobes (Wykes et al. 2013; Eilek 2014),

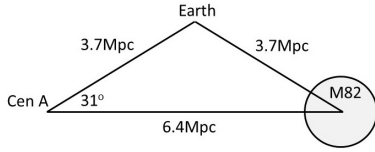


**Figure 1.** Geometry of Centaurus A, M82 and the Earth.

suggests a larger energy input in the past (iii) previous enhanced activity is consistent with a history of galaxy mergers in the past 1-2 Gyr (Wang et al 2020).

In the next section we explore this model further with the use of Monte Carlo calculation of a burst of UHECR emitted by Cen A, encountering a sphere of enhanced scattering representing the M81 group, and propagating from there to a detector at the Earth.

## 2 AN ILLUSTRATIVE MONTE CARLO CALCULATION

We use a Monte Carlo model of small angle UHECR scattering to examine the possibility that the TA hotspot is due to enhanced scattering by the M81 group of galaxies and principally by the halo of M82. Given the uncertainty in crucial parameters the model is illustrative rather than definitive. Many detailed variants of our basic model might be considered.

Our picture is that the lobes of Cen A act as a reservoir of UHECR (Matthews et al 2018, 2019, 2020). UHECR are injected into the reservoir over a period of  $\sim 4$  Myr and varying in time as a Gaussian with  $\sigma = 2$  Myr. UHECR then leak out of the reservoir with an exponential decay time of 3 Myr. The decay time is very uncertain since it depends on UHECR in magnetic field with an unknown structure. Our decay time of 3 Myr is chosen to reproduce the observed ratio of the Cen A and M82 hotspots as shown in figure 2. It is consistent with, if somewhat shorter than, the estimates made by Matthews & Taylor (2021). In the calculation, the time  $t = 0$  corresponds to the peak in UHECR production by Cen A. The UHECR arriving at the Earth via M82 are delayed  $\sim 20$  Myr relative to those arriving by direct propagation from Cen A. We ignore GZK and other losses since they occur on a longer timescale.

We treat the UHECR as monoenergetic with a uniform scattering rate outside the halo of M82. The scattering rate is chosen to give an approximate match to the rather uncertain angular size of the PAO hotspot coinciding with Cen A. The monoenergetic assumption is a good representation because the UHECR energy spectrum is steep and dominated by UHECR with energies close to the lower energy cut-off. Some UHECR arrive directly at the Earth. Other UHECR are scattered by M82 halo to arrive at the Earth from the direction of M82. We adopt the geometry shown in figure 1 where the distance of both Cen A and M82 from the Earth is 3.7 Mpc. The distance between Cen A and M82 is 6.4 Mpc. The spherical halo of enhanced scattering around M82 has a radius of 800 kpc.

A sphere of enhanced scattering represents the halo of M82. The sphere is placed on the horizontal  $z$  axis, thus imposing cylindrical  $(r, z)$  symmetry on the calculation. The enhanced scattering rate in the halo is chosen to be forty times that in the intergalactic medium. This is sufficient to make the scattering sphere optically thick to UHECR. The scattering rate determines how far the UHECR penetrate into the sphere before reflection back to the surface. Its value makes little difference to the results provided optical thickness is maintained. We add a notional detector at the position of the Earth

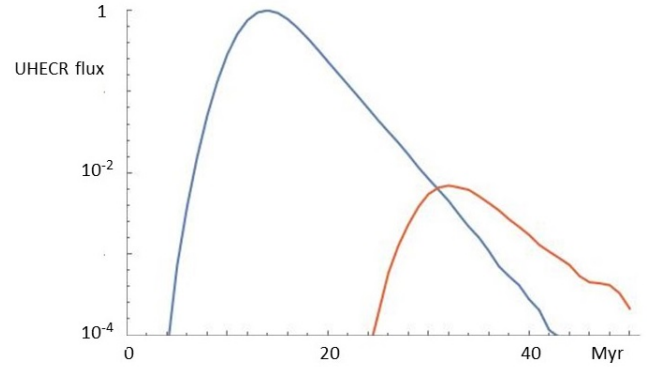


**Figure 2.** Time evolution of the logarithmic UHECR intensity at the Earth (i) UHECR arriving directly from Centaurus A without passing through the halo of M82 (blue line) (ii) UHECR arriving at the Earth having passed through the halo of M82 (brown line).

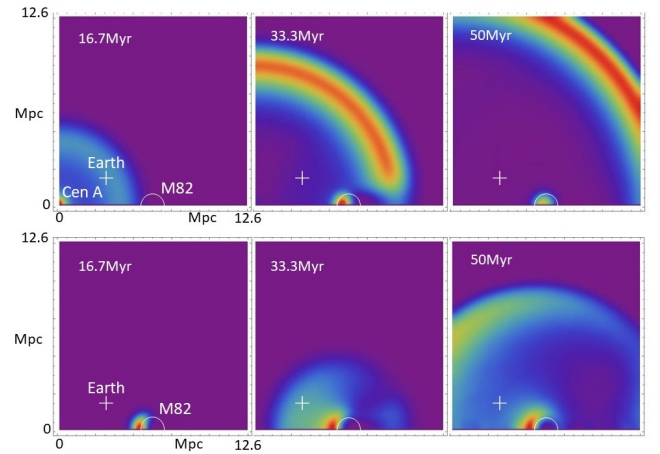


**Figure 3.** The top row gives the density plotted in  $(r, z)$  of all UHECR at times 16.7, 33.3 and 50 Myr. The bottom row is the density of only UHECR that have at some time in their prior history passed through the halo of M82 but are not at present within the halo. In each plot the colour scales are scaled to the maximum UHECR density. The absolute scaling can be deduced from Figure 2.

and analyse how the UHECR number density and anisotropy evolve in time.

The UHECR density in  $(r, z)$  is plotted in figure 3. The shell of UHECR expanding away from Cen A can be clearly seen. The number of UHECR reflected by M82 is smaller and is not easily seen in the top row of figure 3 apart from those within the M82 halo. The bottom row of figure 3 plots only those UHECR that have (i) passed through the halo of M82, and (ii) are not at present within the halo. The intensity of reflected UHECR is stronger in the direction back towards Cen A with a broad spread in angle that encompasses the Earth.

Figure 4 plots the angle of the mean streaming velocity of UHECR arriving at the Earth. The angle is defined relative to the  $z$  axis connecting Cen A to M82. As expected, the angle initially corresponds to arrival from the direction of Cen A and then swings round to point at M82 when the reflected UHECR arrive.

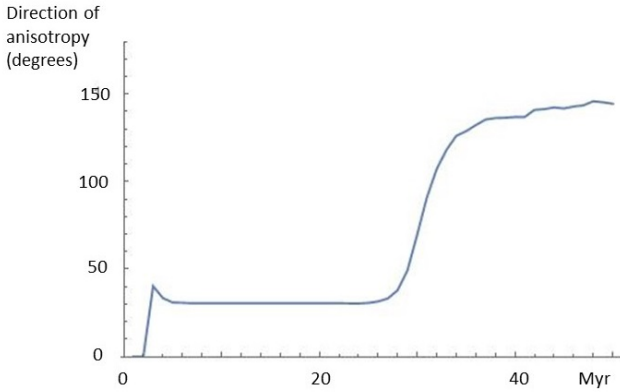


**Figure 4.** The angle in degrees of the direction of anisotropy at the Earth. The angle is defined relative to the  $z$  axis joining CenA and M82 such that Cen A lies at angle  $31^\circ$  and M82 at angle  $149^\circ$ .

### 3 ENERGETICS

The UHECR fluxes from M82 and Cen A are roughly comparable at the present time. Figure 2 therefore suggests that the flux from Cen A  $\sim 20$  Myr ago needs to have been  $\sim 200$  times greater than at present if the flux of UHECR reflected from M82 is to have its present value. In this section, we examine whether this is reasonable.

From figure 4 of di Matteo et al (2019) we make the very approximate estimate that UHECR with energies above 53EeV arrive at the Earth from the M82 hotspot with an excess above the background at the rate of  $\sim 5 \times 10^{-21} \text{cm}^{-2} \text{s}^{-1}$ . This estimate depends heavily on how a line is drawn around the complicated structure and fuzzy extent of the hotspot. If the arrival rate directly from Cen is 200 times greater than the arrival rate via M82, the UHECR luminosity of Cen A 20 Myr ago would have been approximately  $1.4 \times 10^{41} \text{erg s}^{-1}$ . This is  $2 \times 10^{-5}$  of the Eddington luminosity of  $7 \times 10^{45} \text{erg s}^{-1}$  for a Cen A black hole mass of  $5.5 \times 10^7 M_\odot$  (Cappellari et al 2009). Assuming that 10 percent of the Cen A Eddington luminosity was given to CR with energies above 1GeV, a CR spectral index of -2.3 between 1GeV and 50EeV would provide the required UHECR luminosity of the TA hotspot. An efficiency of 10 percent and a spectral index of -2.3 is consistent with the efficiency and spectrum of CR production by high velocity shocks in supernova remnants (Bell et al 2019).

We therefore conclude that energy and power considerations are consistent with a model in which the M82 UHECR hotspot is an echo from Cen A.

### 4 IMPLICATIONS FOR COMPOSITION

UHECR released into the IGM by Cen A are comprised of a range of energies, and probably also a range of charges  $Ze$ . UHECR arriving at the Earth with the same energy may have high different  $Z$  and different scattering rates in the intergalactic medium, and hence different degrees of anisotropy. An additional complication in our model is that UHECR arriving via M82 and directly from Cen A have a different history even if they were accelerated at the same time in Cen A. UHECR with higher  $Z$  but the same energy may be contained for longer within the lobes of Cen A in contrast to low  $Z$  particles that escape more easily. Hence, UHECR arriving via M82 might be expected to have a lower  $Z$  than those escaping later and arriving at the Earth directly from Cen A.

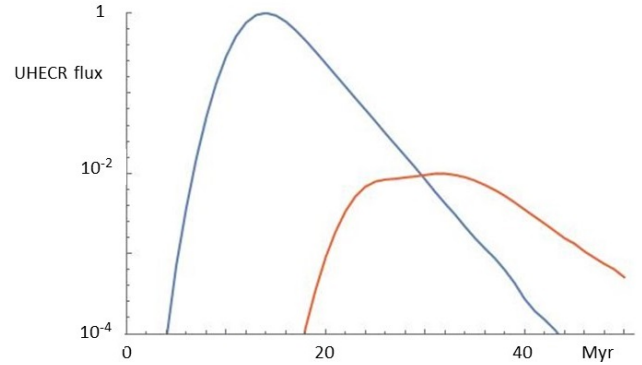


**Figure 5.** Time evolution of the logarithmic UHECR flux at the Earth (i) UHECR arriving directly from Centaurus A without passing through a starburst halo (blue line) (ii) UHECR arriving at the Earth having passed through the haloes of M82, NGC253 or IC342 (brown line).

It would be consistent with the Matthews & Taylor (2021) estimates of UHECR escape times from radio galaxies for 50EeV protons to escape in a few Myr but for higher  $Z$  nuclei to leak out on the timescale of 20Myr. If this applies to Cen A, the ratio of the flux from M82 to the direct flux from Cen A may represent the relative production rates 20Myr ago of light and intermediate mass UHECR nuclei. It will be interesting to see whether this conjecture is confirmed by further data and refinements in the analysis of UHECR composition.

### 5 ECHOES FROM OTHER STARBURST GALAXIES

We now add other strong nearby starburst galaxies to the model to explore their contribution to the UHECR sky. From Table 4 of Ackermann et al we add NGC253 and IC342 at distances of 2.5 and 3.7Mpc respectively from Earth. We do not include the strong starburst galaxy NGC4945 which is part of the Centaurus A group of galaxies and separated from Cen A by a distance of only 480kpc (Tully et al 2015) which is comparable with the spatial extent of the lobes of Cen A. UHECR reaching Earth from NGC4945 and Cen A are not separable either in angle on the sky or in their travel times to the Earth. Any attempt to realistically model CR propagation through NGC4945 would add considerable complexity to the calculation without making much difference to the results.

The starburst galaxy M83 is also a member of the same group of galaxies as Cen A but at a greater distance from Cen A than NGC4945. We tried including M83 in our model according to the same formalism adopted for NGC253 and IC342 and found that it made little difference to the results. For simplicity and because of the modelling uncertainties we also omit M83 from the results presented here.

NG253 and IC342 have radio luminosities at 1.4GHz that are smaller than that of M82 by factors of 0.39 and 0.35 respectively (Ackermann et al 2012) and we assume that their UHECR reflectivities are smaller by the same ratios. We model this rather arbitrarily by reducing the areal cross-sections of their haloes. The radii of their haloes are consequently taken to be  $800 \times \sqrt{0.39}$  and  $800 \times \sqrt{0.35}$  kpc respectively. In other respects we model NGC253 and IC342 in the same way as M82.

Figure 5 is a plot against time of the UHECR flux from Cen A (blue line) and the combined flux at the Earth of UHECR reflected from the haloes of the three starburst galaxies. Comparison with Figure 2

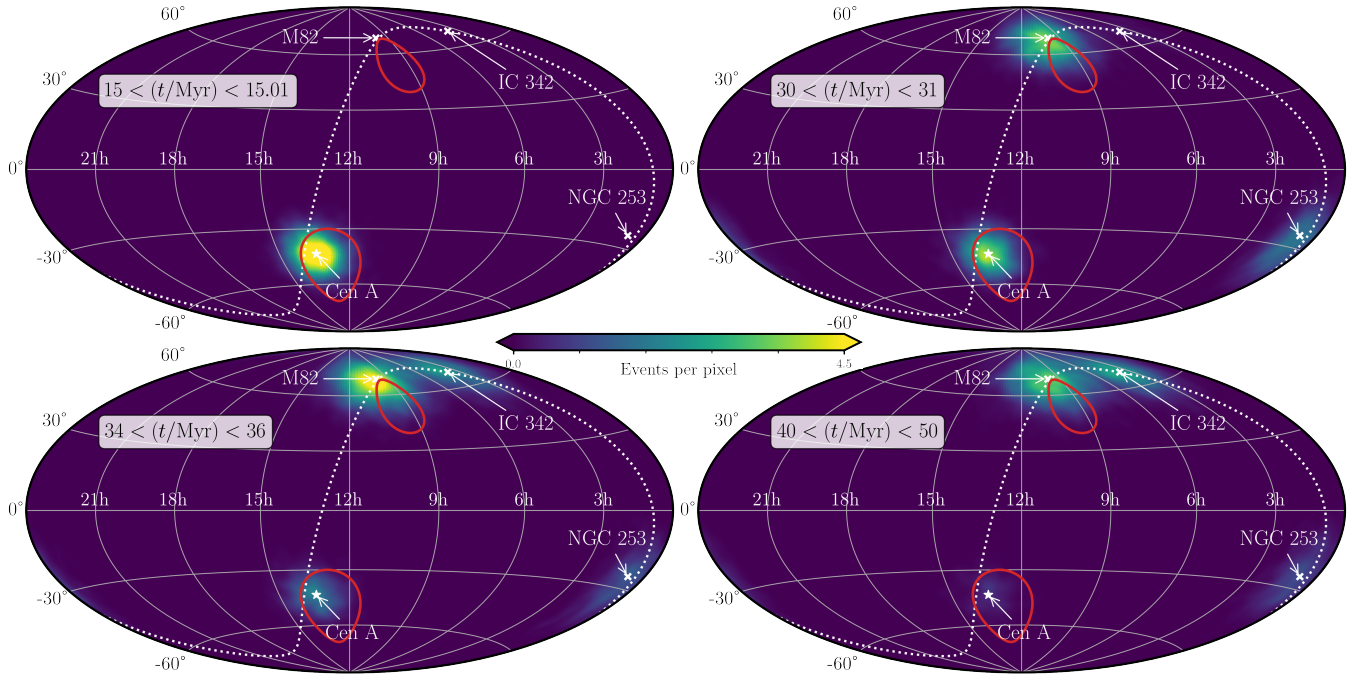


**Figure 6.** All-sky Hammer projection plot in equatorial coordinates (right ascension and declination) of arrival directions of Monte Carlo particles in four time bands of different duration:  $15.0 < t < 15.01\text{Myr}$  (Top Left),  $30 < t < 31\text{Myr}$  (Top Right),  $34 < t < 36\text{Myr}$  (Bottom Left),  $40 < t < 50\text{Myr}$  (Bottom Right). The three starburst galaxies included in the calculation (M82, NGC253 & IC342) are labelled, as is Cen A, and the red lines mark the approximate positions of the TA and PAO excesses in the northern and southern hemispheres, respectively (Di Matteo et al. 2019). The plot is produced using Healpy, a python implementation of the HEALpix scheme (Górski et al 2005; Zonca et al 2019). The colour-scale encodes the number of particles per HEALpix pixel, initially calculated with  $64 \times 64$  pixels covering the sky, which has then been smoothed with a Gaussian symmetric beam with full-width at half-maximum of  $5^\circ$ . The colour-map can be thought of as a linear measure of UHECR intensity at Earth. The  $34 < t < 36\text{Myr}$  plot provides a reasonable qualitative match with the combined TA and PAO map from Di Matteo et al. (2019; see their figure 4).

gives a comparison of the fluxes from NGC253 and IC342 relative to that from M82.

The inclusion of NGC253 and IC342 disrupts the cylindrical symmetry of the calculation and we present the results as all-sky plots. Figure 6 plots the arrival directions of UHECR in equatorial coordinates in three time bands: (A)  $15.0 < t < 15.01\text{Myr}$  (Top Left), close to the peak in the direct flux from Cen A (B)  $30 < t < 31\text{Myr}$  (Bottom Left), (C)  $34 < t < 36\text{Myr}$  (Bottom Left), close to the peak in the flux from haloes (D)  $40 < t < 50\text{Myr}$  (Bottom Right), when the direct flux from Cen A has died down. The choice of different time intervals scales the flux at the different times by the ratios 1:100:200:1000 respectively, thus allowing the same colour scaling to be used on each plot. The all-sky plot uses the Hierarchical Equal Area isoLatitude Pixelization (HEALpix<sup>1</sup>) scheme, so that Monte Carlo particles are binned according to which HEALpix pixel they fall into, with  $64 \times 64$  pixels covering the sky.

Comparison with Figure 4 of di Matteo (2019) shows best agreement with the combined TA and PAO data in time band (C) at  $t \approx 35\text{Myr}$ . The actual timing and the ratio between the direct and echoed fluxes depends on the escape time of 3Myr chosen in our calculation. Nevertheless, figure 6 demonstrates that the Monte Carlo model is able to reproduce the TA and PAO fluxes when we choose our parameters suitably.

The TA and PAO data show UHECR arriving from a wider range

of directions on the sky. These may be reflections from more distant starburst galaxies of UHECR released by Cen A at earlier times. Reflection may also occur from less prominent star-forming regions in multiple nearby galaxies. Alternatively, UHECR may originate in other radio galaxies such as Fornax A (Matthews et al 2018) or a combination of multiple sources (Hardcastle et al 2010; Eichmann 2019).

## 6 CONCLUSIONS

In summary, we have shown that a viable model can be constructed in which the TA hotspot is an echo of earlier UHECR production by Cen A during a period of greater activity 20Myr ago. The suggested echo is due to enhanced UHECR scattering by the M81 group of galaxies and in particular by the halo of the starburst galaxy M82. Echoes from other starburst galaxies or other regions of enhanced magnetic field may be responsible for UHECR arriving from other parts of the sky. The model has the potential to reconcile the statistical association of UHECR with starburst galaxies and the inability, due to their relatively low power, of starburst galaxies themselves to generate UHECR of sufficient ultra-high energy. Differences in composition may result from the varied histories of UHECR arriving at the Earth by different paths. As more data is collected, UHECR may be used to probe the local intergalactic environment and the structure of starburst haloes out to distances of 10-20 Mpc from the Earth.

<sup>1</sup> <http://healpix.sf.net>

**ACKNOWLEDGMENTS**

We thank Andrew Taylor for helpful discussions. ARB acknowledges the support of an Emeritus Fellowship from the Leverhulme Trust. JM acknowledges a Herchel Smith Fellowship at the University of Cambridge. Some of the results in this paper have been derived using the healpy and HEALPix packages (Górski et al 2005; Zonca et al 2019). We also gratefully acknowledge the use of Astropy, a community-developed core Python package for astronomy (Astropy Collaboration 2013, 2018), and Matplotlib v3.1.1 (Hunter 2007). The Monte Carlo calculations were performed using the computing resources provided by STFC Scientific Computing Department's SCARF cluster.

**DATA AVAILABILITY**

The data underlying this article are available from the authors on reasonable request.

**REFERENCES**

- Aab A et al (Pierre Auger collaboration) 2018 *ApJ* 853, L29  
 Abbasi RU et al (The Telescope Array Collaboration) 2018 *ApJ* 867, L27  
 Ackermann M et al 2012 *ApJ* 755, 164  
 Aharonian FA, Belyanin AA, Derishev EV, Kocharovskiy VV, Kocharovskiy VIV 2002 *Phys Rev D* 66, 023005  
 Alves Batista et al 2019 *Frontiers Astr Space Sci* 6,23  
 Anchordoqui LA 2017, *Proc European Physical Society Conf. on High Energy Physics (EPS-HEP2017)*, Venice, Italy. p. 1, <http://adsabs.harvard.edu/abs/2017hep.confE...1A>  
 Anchordoqui LA 2018 *Phys Rev D* 97, 063010  
 Astropy Collaboration, 2013, *A&A*, 558, A33.  
 Astropy Collaboration, 2018, *AJ*, 156, 123.  
 Baerwald P, Bustamente M, Winter W 2015 *Astropart Phys* 62, 66  
 Beckmann RS et al 2019 *A&A* 631, A60  
 Bell AR, Araudo AT, Matthews JH, Blundell KM 2018 *MNRAS* 473, 2364  
 Bell AR, Matthews JH, Blundell KM 2019 *MNRAS* 488, 2466  
 Bister T et al, (Pierre Auger Collaboration) 2021 *Phys Scripta* 96, 074003  
 Blandford RD 2000 *Physica Scripta* T85, 191  
 Boncioli D, Biehl D, Winter W 2019 *ApJ* 872, 110  
 Cappellari M, Neumayer N, Reunanen J, van der Werf P, de Zeeuw PT, Rix H-W 2009 *MNRAS* 394, 660  
 Cavagnolo KW, McNamara BR, Nulksen PEJ, Caroilla CL, Jones C, Birzan L 2010 *ApJ* 720, 1066  
 de Cea del Pozo E, Torres DF, Marrero AYR 2009 *ApJ* 698, 1054  
 Dermer CD 2011 *AIPC* 1516, 252D  
 di Matteo A et al 2019 *Proc International Cosmic Ray Conf (ICRC)* 36, 439  
 Domingo-Santamaria E, Torres DF 2005 *A&A* 444, 403  
 Eilek JA 2014 *New J Phys* 16, 045001  
 Eichmann B, Rachen JP, Merten L, van Vliet A, Becker Tjus J 2018 *JCAP*02(2018)036  
 Eichmann B 2019, *Proc International Cosmic Ray Conf (ICRC)* 36, 245  
 Eilek JA 2014 *New J Phys* 16,045001  
 Gaspari M, Temi P, Brighenti, F 2017 *MNRAS* 466, 677  
 Górski KM, Hivon E, Banday AJ, Wandelt BD, Hansen FK, Reinecke M, Bartelmann M, 2005, *ApJ* 622, 759  
 Greisen K 1966 *Phys Rev Lett* 16, 748  
 Guedes Lang R, Taylor AM, Ahlers M, de Souza V, 2020, *Phys.Rev.D* 102, 063012  
 Hardcastle MJ, Cheung CC, Feain IJ, Stawar L, 2009 *MNRAS* 393, 1041  
 Hardcastle MJ, 2010, *MNRAS*, 405, 2810  
 Heckman TM, Armus L, Miley GK 1990 *ApJS* 74, 833  
 Heinze J, Biehl D, Fedynitch A, Boncioli D, Rudolph A, Winter W 2020 *MNRAS* 498, 5990  
 Hillas AM 1984 *ARAA* 22, 425  
 Hooper D, Sarkar S, Taylor AM 2007 *Astropart Phys* 27, 113  
 Hunter JD 2007, *Comput. Sci. Eng.*, 9, 90  
 Joshi JC, Mirand LS, Razzaque S, Yang L 2018 *MNRAS* 478, L1  
 Kawata K et al 2015 *Proc ICRC2015*, 276  
 Lemoine M, Pelletier G 2010 *MNRAS* 402, 321  
 Lovelace RVE 1976 *Nature* 262,649  
 Mackie G, Fabbiano G 1998 *AJ* 115, 514  
 Maccagni FM, Murgia M, Serra P, Govoni F, Morokuma-Matsui K, Kleiner D, Buchner S et al 2020, *A&A*, 634, A9  
 Massaglia S 2007 *Nucl Phys B Proc Suppl* 165, 130  
 Matthews JH, Bell AR, Blundell KM, Araudo AT 2018 *MNRAS* 479, L76  
 Matthews JH, Bell AR, Blundell KM, Araudo AT 2019 *MNRAS* 482, 4303  
 Matthews JH, Bell AR, Blundell KM 2020 *New Astronomy Reviews*, 89, 101543  
 Matthews JH, Taylor AM 2021 *MNRAS* 503.5948  
 O'Sullivan S, Reville B, Taylor AM 2009 *MNRAS* 400, 24  
 Persic M, Rephaeli Y 2020 *MNRAS* 491, 5740  
 Ptitsyna V, Troitsky SV 2010 *Phys Usp* 53, 691  
 Romero GE, Muller AL, Roth M 2018 *A&A* 616, A57  
 Rudolph A, Bosnjak Z, Palladino A, Sadeh I, Winter W 2021 *arXiv:210704612*  
 Russell HR, McNamara BR, Edge AC, Hogan MT, Main RA, Vantghem AN 2013 *MNRAS* 432, 530  
 Samuelsson F, Begue D, Ryde, Pe'er A 2019 *ApJ* 876, 93  
 Stecker FW, Salamon MH 1999 *ApJ* 512, 521  
 Tully BR, Libeskind NI, Karachentsev IG, Karachentseva VE, Rizzi L, Shaya EL 2015 *ApJ* 802 L25  
 van Velzen S, Falcke H, Schellart P, Nierstenhofer N, Kamper K-H 2012 *A&A* 544, A18  
 Wang J, Hammer F, Rejbuka M, Crnojevic D, Yang Y 2020 *MNRAS* 498, 2766  
 Waxman E 1995 *PRL* 75, 386  
 Waxman E, Bahcall JN 1997 *Phys Rev Lett* 78, 2292  
 Waxman E, Bahcall JN 1998 *Phys Rev D* 59, 023002  
 Wilde MC et al 2021 *ApJ* 912:9  
 Wykes et al 2013 *A&A* 558, A19  
 Yang H-Y K, Reynolds CS 2016 *ApJ* 829, 90  
 Zatsepin GT, Kuz'min VA 1966 *Sov J Expt Theor Phys Lett* 4, 78  
 Zhang BT, Murase K, Kumra SS, Horiuchi S, Meszaros P 2016 *Phys Rev D* 97, 083010  
 Zonca A, Singer L, Lenz D, Reinecke M, Rosset C, Hivon E, Górski KM 2019 *The Open Journal* 4, 1298